"One Stone, Two Birds": Engineering 2-D Ultrathin Heterostructure Nanosheet BiNS@$NaLnF_4$ for Dual-Modal Computed Tomography /Magnetic Resonance Imaging-guided, Photonic Synergetic Theranostics

Sihan Ma[§,⊥], Lin Wang[*,※,‡], Zongjunlin Liu[‡], Xian Luo[‡], Zonglang Zhou[‡,□], Jun Xie[‡], Yipeng Li[§,⊥], Shuo Cong[§,⊥], Ming Zhou[†], Yang Xu[*,†] and Guang Ran[*,§,⊥]

[§]College of energy, Xiamen University, Xiamen city, Fujian Province, 361002, China

[‡] School of Medicine, Xiamen University, Xiamen, Fujian, China

[※]Department of Oncology, Zhongshan Hospital, Xiamen University, No. 201-209 Hubinnan Road, Xiamen 361004, Fujian Province, China

[†]School of pharmaceutical sciences, Xiamen University, Xiamen city, Fujian Province, 361002, China

[⊥]Fujian Research Center for Nuclear Engineering, Xiamen City, Fujian Province, 361102, China

[□]174 Clinical College affiliated to Anhui Medical University, Anhui Medical University, Hefei, Anhui Province, 230032, China

Supplementary Materials

1. Materials and methods

2.1 Materials

Analytical grade $Bi(NO_3)_3 \cdot 5H_2O$ (99%), $Yb(NO_3)_3 \cdot 6H_2O$ (99%), $Er(NO_3)_3 \cdot 6H_2O$ (99%), $Gd(NO_3)_3 \cdot 6H_2O$ (99.99%), $Ce(NO_3)_3 \cdot 6H_2O$ (99%), ethylene glycol ($C_2H_6O_2$, 500 mL, 99%), KCl (99%), NH_4F (99%) and polyvinyl pyrrolidone PVP were purchased from Aladdin Reagents (Shanghai, China).

1.2 Synthesis of BiNS@$NaLnF_4$ (Ln=Gd/Er,Yb,Ce)

Bismuth-based nanosheets BiNS were synthesized by a facile solvothermal strategy. A total of 1 mmol $Bi(NO_3)_3$ and 0.5g of PVP (MW=10k) were dissolved into 35 mL ethylene glycol (EG) with deionized water (DI) (EG:DI=5:2) to form transparent solution **A** under vigorous stirring at room temperature for 10 min. KCl (0.04g) was dissolved into 10 mL EG to form a transparent solution **B** under vigorous stirring with ultrasound at room temperature for 10 min. Then, solution **B** was slowly mixed in solution **A**, to form a homogeneous mixture **C** under stirring at room temperature. Subsequently, mixture **C** was transferred into a 50mL reaction vessel and heated at 160℃ for 24 h. After reaction, the system was naturally cooled to room temperature. The milk-white products were collected under centrifugation at 8000 rpm (6578 gravity) for 3 min and washed with DI and ethanol three times or more to remove other residues.

The as-prepared BiNSs in 10 mL EG were added to a 50 mL beaker. Subsequently, 30

mL of EG with $Gd(NO_3)_3$ (0.1 mmol), $Yb(NO_3)_3$ (0.1 mmol), $Er(NO_3)_3$ (0.02 mmol), $Ce(NO_3)_3$ (0.02 mmol), 10 mL DI and 10 mmol NaF were slowly added into the above solution and stirred continually at room temperature for 10 min. Finally, the mixture was sealed into an autoclave and reacted at 100℃for 4 h. The sample was collected after the system was naturally cooled to room temperature and further washed with DI and alcohol three times or more, and UV-light irradiation durations (λ=365 nm), the pure products BiNS@$NaLnF_4$ were collected after centrifugation at 8000rpm and freeze drying.

In addition, a hollow heterojunction nanomaterial BiNPs@$NaLnF_4$ was controllably synthesized, following above steps. Noticeably, no DI was required for the whole fabrication process.

1.3 Characterization

The crystal structures and phase feature of the samples were determined by powder X-ray diffraction (XRD, Rigaku Ultima IV) with Cu Kα radiation with an operation voltage and current maintained at 40 kV and 30 mA, respectively. The size and morphology of the samples were analyzed by scanning electron microscope (SEM, Hitachi S-4800, Japan) with an operation voltage at 300 kV and low/high resolution lanthanum hexaboride transmission electron microscope (TEM, TECANI G20 F30 TWIN, Oxford) with an electron-emission gun operation voltage at 200 kV. Fourier transform infrared spectroscopy (FTIR, Thermo Scientific Nicolet Is5 spectrometer, USA) was performed to determine the functional groups on the surface of the products. The elemental analysis of nanoparticles were determined by obtaining the energy

dispersive spectrum (EDS) from TEM that containing the map scanning analysis. Dynamic light scattering (DLS, Brookhaven Instruments-Omni, USA) was used to analyze the size distribution of products in different solution.

1.4 Band structure and DFT calculation of BiNS@$NaLnF_4$

All the calculations were performed at the correction functions generalized gradient approximation (GGA) functional of the Perdew–Burke–Ernzerhof (PBE) level with the plane wave of Norm-conserving pseudopotential implemented in the package sequential total energy package (CASTEP). The energy cutoff of the plane wave function was set to 340 eV and the Brillouin zone was integrated using the Monlhorst-Pack K point grid which was set to be 4×4×2. The band structure and density of states (DOS) were calculated in this process.

1.5 Biosafety and cellular uptakes of BiNS@$NaLnF_4$

Cell line and cell culture: a human cervical cancer cell line (HeLa) was purchased from Chinese Academy of Medical Sciences Union Hospital cell bank. The cells were cultured in an animal cell culture media medium (MEM, HyClone, USA) in a humidified incubator at 37℃ and 5% CO_2 and the culture medium was replaced every 24h.

The cytocompatibility of the BiNS@$NaLnF_4$ was investigated by a traditional in vitro MTT assay on HeLa. The cells were cultured under a humidified incubator at 37℃ and 5% CO_2. The cells were seeded in 96-well plates at a density of ~5000 cells per well and were cultured for 24 h. Different concentrations of BiNS@$NaLnF_4$ (0, 25, 50, 100, 200 μg mL^{-1}) were mixed to the 96-well plates containing the cells and MTT solution

was used to detect cell survival rate in vitro at wavelength 570 nm.

The *in vitro* cell experiments: the esophagus cancer (ECA109) cells were cultured and incubated with different concentration samples (BiNS@$NaLnF_4$, 0-200 μg mL^{-1}) with or without light irradiation (visible light - NIR laser) for different times (5-10 min). The cellular uptakes generation of ROS strategies were carried out, a simulative visible light (300 W Xeon light, $\lambda > 400$ nm) was applied as a light source. The corresponding cell viabilities were obtained by MTT methods after laser irradiation.

Stability of as-prepared samples were analyzed by dynamic light scatter instrument, the size distribution in water, phosphate-buffered saline (PBS, pH 7.4) were recorded, respectively.

1.6 Photothermal conversion of BiNS@$NaLnF_4$

A 980nm laser treatment has obvious application advantages compared with 808nm in clinical application, because, among other things, it has a good penetrability. To achieve the photothermal conversion under 980 nm laser irradiation, BiNS@$NaLnF_4$ were exploited as a photothermal agent at 980 nm laser instrument in the following research, which was based on the dramatic absorption of near- infrared (NIR) light absorption law and used the photothermal effect principle to detect the photothermal transfer efficiency (η). The corresponding liner relationship of time versus, and the between relationship temperature and concentration were recorded. The photothermal conversion efficiency (η) of BiNS@$NaLnF_4$ can be calculated according to the following equation in previous reports[1, 2].

$$\eta = \frac{hA(\Delta T_{\max,sample} - \Delta T_{\max,H_2O})}{I(1-10^{-A_\lambda})}$$

Where h is the heat transfer coefficient, A is the surface area of the laser irradiated container, $\Delta T_{max,sample}$ and $\Delta T_{max,H2O}$ are the temperature change of BiNS@$NaLnF_4$ dispersion and solvent (DI), respectively, at the maximum steady state temperature. I is the laser instrument power density, A_λ is the absorbance of BiNS@$NaLnF_4$ solution at wavenumber 980 nm laser. The detailed calculation for the equations are shown in the supporting information.

1.7 *in vitro* X-ray CT and MRI

CT phantom images of different concentrations (0, 1.25, 2.5, 5.0 and 10 mg mL^{-1}) of nanoparticles and commercial Ioversol were recorded by X-ray CT imaging using Siemense Inveon PET/CT with voltage of 80 kV and current maintained at 88 μA. MRI measurements were carried out on a 9.4 T/30 cm micro Bruker Biospec scanner (Esslingen, Germany) equipped with actively shielded gradients. The T_1-weighted relaxivities ($R_1=1/(T_1 \cdot \text{concentration})$) data of the interesting regions were calculated, and the corresponding relaxation time were measured in the present experiment.

1.8 Detection of free radicals ROS

The possibility of visible-light to induce •OH and $•O^{2-}$ generation from BiNS was evaluated using traditional pollutant, methyl orange (MO) assay, which can be degraded by $•O^{2-}$ or •OH. The concentration of 0.4 mg mL^{-1} MO aqueous solution was used to demonstrate the performance of ROS, the different concentrations of BiNS and BiNS@$NaLnF_4$ solution, the same amount of matrix BiNS for BiNS@$NaLnF_4$, were mixed with as-prepared MO solution before visible-light irradiation. Subsequently, the above mixture was treated for 60 min at vis-light irradiation, the irradiated mixture was

collected and centrifuged to store the liquid supernatants, UV-vis-NIR instrument was used to perform the absorption spectra of supernatants. The characteristic absorption peak intensities of MO after irradiation were consistent with the generation of free radicals with different concentrations of BiNS and BiNS@$NaLnF_4$.

To further evaluate the generation of ROS when BiNS@$NaLnF_4$ irradiated, the 2',7'-dichlorofluoresceindiacetate (DCFH) was used as ROS probe. Briefly, 1 mL of BiNS@$NaLnF_4$ (300 ug mL^{-1}) containing 100 μL of DCFH dissolved in PBS (10x) was exposed to visible-NIR irradiation for different period of time. And the results were analyzed by fluorescence spectrometer.

1.9 The animal experiments

The bio-imaging was performed by using Kunming mice (about 25 g) for CT, before imaging, the BiNS@$NaLnF_4$ solution was injected via tail vein (50 mg kg^{-1}). The ECA109-bearing nude mice (BALB/C) were used to perform the photothermal imaging, the samples of the concentration of 0.3 mg mL^{-1} (BiNS@$NaLnF_4$, 50 μL) were injected via intratumorally, and treated under 980 nm laser irradiation with 1.17 W cm^{-2} density for 3 min. For PTT, four groups BALB/C were employed to perform the goals: (a) PBS (b) PBS+laser irradiation (c) BiNS@$NaLnF_4$ (d) BiNS@$NaLnF_4$+laser irradiation, the different groups mice were administrated with 50 μL (0.3 mg mL^{-1}) solution of products via intratumoral injection for three times. The group (b) and (d) were treated with 980 nm NIR laser (1.17 W cm^{-2}, 10 min). Following each treatment, the data of relative tumor volumes and body weight in each group were recorded over the course of 15 day.

1.10 Statistics

The significance of group differences for normally distributed data was assessed by one-way ANOVA followed by Tukey *post hoc* tests. $P < 0.05$ was considered to be statistically significant. The data of X-ray-CT were collected by self-contained software associated with the instrument. The data of particles size distribution were collected and analyzed by the nano-measurement software. The other data in the present paper were calculated by software Origin 8.1. The theoretical calculations data were performed by software Material Studio 7.0 (MS).

Calculation of the photothermal conversion efficiency

The photothermal conversion efficiency of BiNS@$NaLnF_4$ was calculated according to previous reports[1, 2]. The detailed calculation was carried out via the following equations:

First of all, the total energy balance relationship of the system was determined as follows:

$$\sum_i m_i C_{p,i} \frac{dT}{dt} = Q_{BiNPs} + Q_{DI} - Q_{loss} \qquad (1)$$

where m and C_p are the mass and heat capacity constant, respectively. The subscript symbol "i" for m and C_p refers to the solvent (DI) or dispersed matter (BiNS@$NaLnF_4$ nanoparticles). T is the solution temperature at different times. Q_{BiNPs} is the photothermal energy absorbed from the BiNS@$NaLnF_4$ per second. Q_S is the heat associated with the light absorbed by DI per second. Q_{loss} is the heat which released into the surrounding atmosphere.

$$Q_{BiNPs} = I(1-10^{-A\lambda})\eta \qquad (2)$$

$$Q_{loss} = hA\Delta T \qquad (3)$$

where I is the near infrared laser instrument power density, A_λ is the absorbance of the BiNS@$NaLnF_4$ at the wavelength 980 nm in aqueous solution, and η is the photothermal conversion efficiency of the BiNS@$NaLnF_4$ which is the ratio of absorbed light energy converting to thermal energy. Where h is the heat transfer coefficient, A is the surface area of the container, and ΔT is the temperature change at different times, which is computed by T-T_{surr} (T and T_{surr} are the solution temperature and ambient temperature of the surrounding, respectively). When the DI is heated, the heat input is equal to the heat output at the maximum steady-statue temperature, so the equation (3) can be described as follows:

$$Q_{loss} = Q_{DI} = hA\Delta T_{\max,H_2O} \qquad (4)$$

For the situation of nanoparticles solution, the total energy absorbed by mixture solution

is equal to the energy loss at the maximum steady-state temperature, so the equation can be:

$$Q_{loss} = Q_{DI} + Q_{BiNPs} = hA\Delta T_{\max,sample} \qquad (5)$$

Where $\Delta T_{max,sample}$ is the temperature change of the BiNS@$NaLnF_4$ dispersion at the maximum steady-state temperature. According to the above equations expression, the photothermal conversion efficiency (η) can be expressed as follows:

$$\eta = \frac{hA(\Delta T_{\max,sample} - \Delta T_{\max,H_2O})}{I(1-10^{-A_\lambda})} \qquad (6)$$

In order to get the multiplying transfer constant h and surface area of the laser irradiated container A , we define number θ, which is introduced as the ratio of ΔT to $\Delta T_{\max}$:

$$\theta = \frac{\Delta T}{\Delta T_{\max}} \qquad (7)$$

Substituting equation (7) into equation (1) and (3), we can obtain:

$$\begin{aligned} &\sum_i m_i C_{p,i} \frac{dT}{dt} = Q_{BiNPs} + Q_{DI} - Q_{loss} = Q_{BiNPs} + Q_{DI} - hA\Delta T \\ &= Q_{BiNPs} + Q_{DI} - hA\theta\Delta T_{\max} = \sum_i m_i C_{p,i} \frac{d(\theta\Delta T_{\max} + T_{surr})}{dt} \end{aligned} \qquad (8)$$

Further simplifying this equation, it can be expressed as:

$$\sum_i m_i C_{p,i} \frac{d(\theta\Delta T_{\max} + T_{surr})}{dt} = \sum_i m_i C_{p,i} \frac{\Delta T_{\max} d\theta + \theta d\Delta T_{\max}}{dt} = Q_{BiNPs} + Q_{DI} - hA\theta\Delta T_{\max}$$

$$\frac{d\theta}{dt} = \frac{1}{\sum_i m_i C_{p,i}} \left[\frac{Q_{BiNPs} + Q_{DI} - hA\theta\Delta T_{\max}}{\Delta T_{\max}} \right] = \frac{hA}{\sum_i m_i C_{p,i}} \left[\frac{Q_{BiNPs} + Q_{DI}}{hA\Delta T_{\max}} - \theta \right] \qquad (9)$$

The Q_{BiNPs}+Q_{DI}=0 after the laser instrument was closed, therefore, equation (9) can be:

$$dt = -\frac{\sum_i m_i C_{p,i}}{hA} \frac{d\theta}{\theta} \qquad (10)$$

$$t = -\frac{\sum_i m_i C_{p,i}}{hA} \ln\theta \qquad (11)$$

$$hA = -\frac{\sum_i m_i C_{p,i}}{t} \ln\theta \; ; \; -\frac{\sum_i m_i C_{p,i}}{dt} d(\ln\theta) = k\sum_i m_i C_{p,i} \qquad (12)$$

Where hA can be calculated by the ratio of linear relationship of time t versus -lnθ. Compared with the solvent (water, 2×10^{-4}kg), mass of the BiNS@$NaLnF_4$ (4×10^{-8}kg) was pretty little. Generally, the specific heat of water is much higher than that of other materials. Thereby, the mass of the BiNS@$NaLnF_4$ will be neglected. $C_{p,H2O}$ was 4.2×10^{3}J $kg^{-1}s^{-1}$, so we can determine that hA is 0.00667.

$$A_\lambda = \varepsilon c \phi \quad (13)$$

Where A_λ is defined as the absorbance of the BiNS@$NaLnF_4$ at the wavelength 980 nm in aqueous solution, ε is the light path of the BiNS@$NaLnF_4$ dispersion (the width of a colorimetric dish in experiment, approximately 1.0 cm) and ϕ is the extinction coefficient of the BiNS@$NaLnF_4$ at the given concentration and 980 nm laser radiation. UV-Vis get the value A_λ=0.118 at a concentration of 0.2 mg mL^{-1} and 980 nm laser irradiation. Now go back to equation (6) again, every parameter is clearlydefined. $\Delta T_{max,sample}$ is 32.69 $\Delta T_{max,H2O}$ is 3.09. I is 2.35 W, where the area of the light spot is approximately 0.5 cm^2. A_λ is 0.307. Thus, the photothermal conversion efficiency (η) of the BiNS@$NaLnF_4$ could be calculated.

Additional information

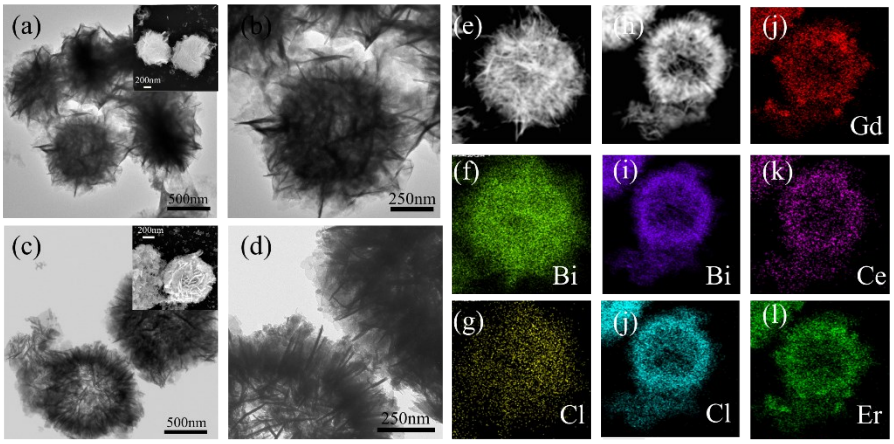

Figure S1 **Characterization of the multi-modal agents Bi-based nanomaterials.** (a)-(d) TEM images of the multi-functional contrast agents BiNPs and BiNPs@$NaLnF_4$ for different magnifying power. Displaying the microstructures and outline of the nanoparticles BiNPs and BiNPs@$NaLnF_4$, respectively. The insert picture is the corresponding SEM images. The map scanning images for BiNPs (e)-(g) and BiNPs@$NaLnF_4$ (h)-(l) illustrate the elemental composition of the products.

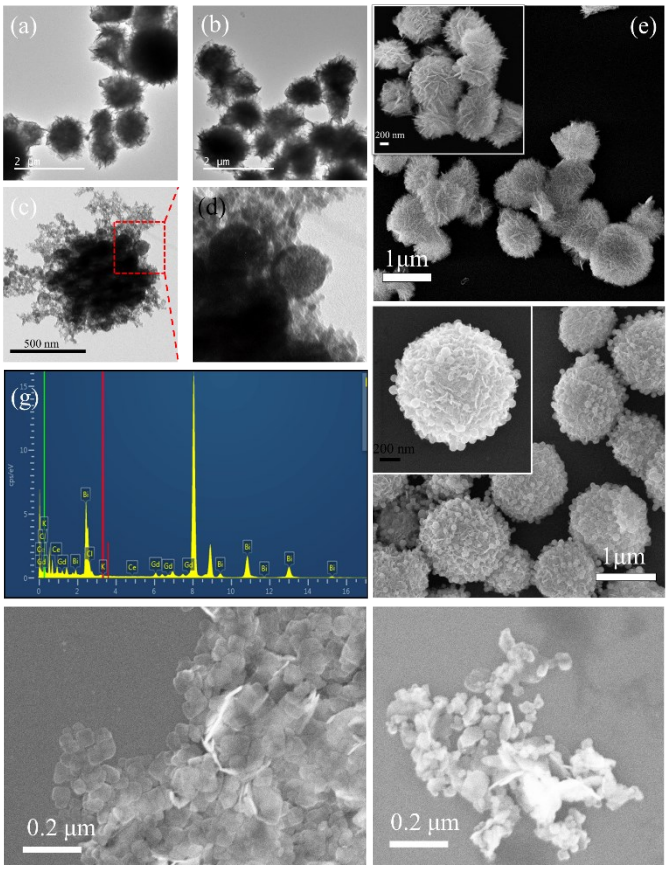

Figure S2 **Images showing the physical morphology of multi-functional contrast agent Bi-based nanomaterials.** TEM distribution images of contrast agents (a)-(b) BiNPs and (c)-(d) BiNPs@$NaLnF_4$, respectively. SEM images of (e) BiNPs and (f) BiNPs@$NaLnF_4$. (g) EDS image of BiNPs@$NaLnF_4$ displays the composition of the nanoparticles. The SEM images of (h) BiNS and (i) BiNS@$NaLnF_4$.

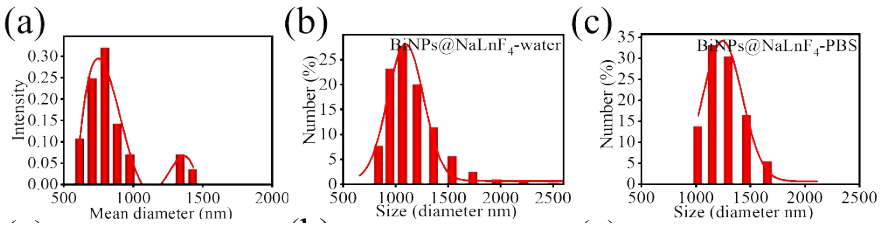

Figure S3 **Size statistics of BiNPs.** (a) Measurements data of BiNPs@$NaLnF_4$ from SEM. (b)-(c) A hydrodynamic distribution was described in the DLS images in DI and the PBS solution for BiNPs@$NaLnF_4$.

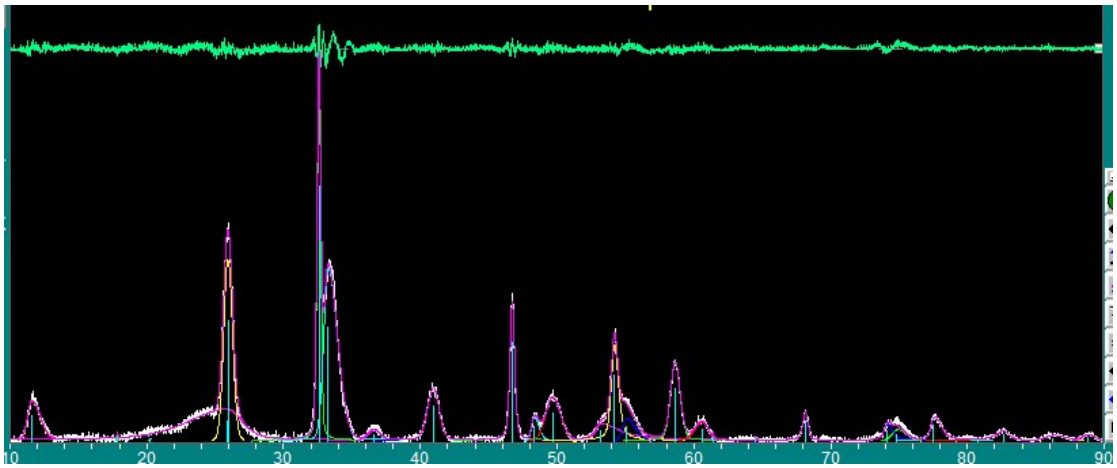

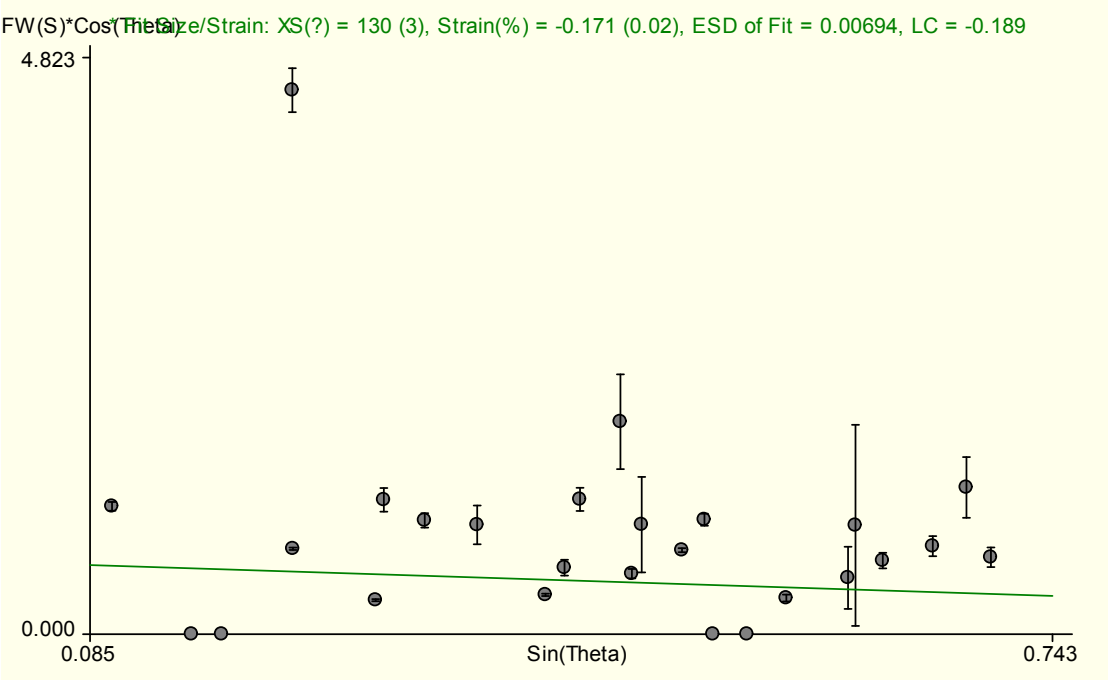

Figure S4 **Refinement fitting for X-ray diffraction structure analysis and the calculation of strain size.**

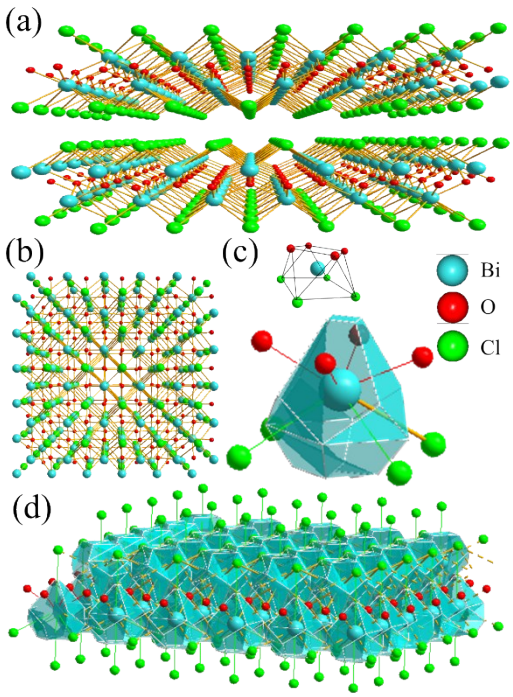

Figure S5 **X-ray diffraction structure analysis of BiOCl.** (a) BiOCl crystal structure viewed along the b axis showing the layers stacked in the direction perpendicular to the c axis. (b) The view of a single layer from c axis. (c) The

coordination geometry of the Bi atom. (d) A single BiOCl crystal structure layer.

Table S1 **Selected atomic bond length information**

Atomic bond	Length(Å)	Atomic bond	Length(Å)
Bi1—O1^{i}	2.3178(7)	Bi1—Cl1^{v}	3.0603(39)
Bi1—O1^{ii}	2.3178(7)	Cl1—Bi1^{vi}	3.0603(39)
Bi1—O1^{iii}	2.3178(7)	Cl1—Bi1^{vii}	3.0603(39)
Bi1—O1	2.3178(7)	Cl1—Bi1^{viii}	3.0603(39)
Bi1—Cl1^{iv}	3.0603(39)	O1—Bi1^{i}	2.3178(7)
Bi1—Cl1	3.0603(39)	O1—Bi1^{ii}	2.3178(7)
Bi1—Cl1^{iii}	3.0603(39)	O1—Bi1^{viii}	2.3178(7)

Table S2 **Selected coordination geometry of crystal bond angles**

Coordination information	Bond angle (^{O})	Coordination information	Bond angle (^{O})
O1^{i}—Bi1—O1^{ii}	114.150(7)	Cl1—Bi1—Cl1^{iii}	78.947(5)
O1^{i}—Bi1—O1^{iii}	72.816(6)	O1^{i}—Bi1—Cl1^{v}	140.498(7)
O1^{ii}—Bi1—O1^{iii}	72.816(6)	O1^{ii}—Bi1—Cl1^{v}	72.805(6)
O1^{i}—Bi1—O1	72.816(6)	O1^{iii}—Bi1—Cl1^{v}	140.498(7)
O1^{ii}—Bi1—O1	72.816(6)	O1—Bi1—Cl1^{v}	72.805(6)
O1^{iii}—Bi1—O1	114.150(7)	Cl1^{iv}—Bi1—Cl1^{v}	78.947(5)
O1^{i}—Bi1—Cl1^{iv}	140.498(7)	Cl1—Bi1—Cl1^{v}	78.947(5)
O1^{ii}—Bi1—Cl1^{iv}	72.805(6)	Cl1^{iii}—Bi1—Cl1^{v}	128.065(5)
O1^{iii}—Bi1—Cl1^{iv}	72.805(6)	Bi1^{vi}—Cl1—Bi1^{vii}	78.947(5)
O1—Bi1—Cl1^{iv}	140.498(7)	Bi1^{vi}—Cl1—Bi1^{viii}	78.947(5)
O1^{i}—Bi1—Cl1	72.805(6)	Bi1^{vii}—Cl1—Bi1^{viii}	128.065(5)
O1^{ii}—Bi1—Cl1	140.498(7)	Bi1vi—Cl1—Bi1	128.065(5)
O1^{iii}—Bi1—Cl1	140.498(7)	Bi1^{vii}—Cl1—Bi1	78.947(5)
O1—Bi1—Cl1	72.805(6)	Bi1^{viii}—Cl1—Bi1	78.947(5)
Cl1^{iv}—Bi1—Cl1	128.065(5)	Bi1^{i}—O1—Bi1^{ii}	114.150(7)
O1^{i}—Bi1—Cl1^{iii}	72.805(6)	Bi1i—O1—Bi1	107.184(8)
O1^{ii}—Bi1—Cl1^{iii}	140.498(7)	Bi1^{ii}—O1—Bi1	107.184(8)
O1^{iii}—Bi1—Cl1^{iii}	72.805(6)	Bi1^{i}—O1—Bi1^{viii}	107.184(8)
O1—Bi1—Cl1^{iii}	140.498(7)	Bi1ii—O1—Bi1viii	107.184(8)
Cl1^{iv}—Bi1—Cl1^{iii}	78.947(5)	Bi1—O1—Bi1viii	114.150(7)
O1—Bi1—Cl1—Bi1^{vi}	38.411(175)	O1—Bi1—O1—Bi1^{i}	0.000(19)
O1—Bi1—Cl1—Bi1^{vi}	-68.920(264)	O1—Bi1—O1—Bi1^{i}	-122.948(17)
O1—Bi1—Cl1—Bi1^{vi}	68.920(264)	O1—Bi1—O1—Bi1^{i}	-61.474(26)
O1—Bi1—Cl1—Bi1^{vi}	-38.411(175)	Cl1—Bi1—O1—Bi1^{i}	-153.455(153)
Cl1—Bi1—Cl1—Bi1^{vi}	180.000(173)	Cl1—Bi1—O1—Bi1^{i}	76.808(101)

Cl1—Bi1—Cl1—Bi1^{vi}	113.647(227)	Cl1—Bi1—O1—Bi1^{i}	30.507(155)
Cl1—Bi1—Cl1—Bi1^{vi}	-113.647(227)	Cl1—Bi1—O1—Bi1^{i}	160.244(101)
O1—Bi1—Cl1—Bi1^{vii}	-27.942(56)	O1—Bi1—O1—Bi1^{ii}	122.948(17)
O1—Bi1—Cl1—Bi1^{vii}	-135.274(88)	O1—Bi1—O1—Bi1^{ii}	-0.000(19)
O1—Bi1—Cl1—Bi1^{vii}	2.567(197)	O1—Bi1—O1—Bi1^{ii}	61.474(26)
O1—Bi1—Cl1—Bi1^{vii}	-104.765(92)	Cl1—Bi1—O1—Bi1^{ii}	-30.507(155)
Cl1—Bi1—Cl1—Bi1^{vii}	113.647(149)	Cl1—Bi1—O1—Bi1^{ii}	-160.244(101)
Cl1—Bi1—Cl1—Bi1^{vii}	47.293(119)	Cl1—Bi1—O1—Bi1^{ii}	153.455(153)
Cl1—Bi1—Cl1—Bi1^{vii}	180.000(138)	Cl1—Bi1—O1—Bi1^{ii}	-76.808(101)
O1—Bi1—Cl1—Bi1^{viii}	104.765(92)	O1—Bi1—O1—Bi1^{viii}	-118.526(18)
O1—Bi1—Cl1—Bi1^{viii}	-2.567(197)	O1—Bi1—O1—Bi1^{viii}	118.526(18)
O1—Bi1—Cl1—Bi1^{viii}	135.274(88)	O1—Bi1—O1—Bi1^{viii}	180.00(2)
O1—Bi1—Cl1—Bi1^{viii}	27.942(56)	Cl1—Bi1—O1—Bi1^{viii}	88.019(154)
Cl1—Bi1—Cl1—Bi1^{viii}	-113.647(149)	Cl1—Bi1—O1—Bi1^{viii}	-41.718(102)
Cl1—Bi1—Cl1—Bi1^{viii}	180.000(138)	Cl1—Bi1—O1—Bi1^{viii}	-88.019(154)
Cl1—Bi1—Cl1—Bi1^{viii}	-47.293(119)	Cl1—Bi1—O1—Bi1^{viii}	41.718(102)

(i) 1-x, 1-y, 1-z; (ii) 1-x, -y, 1-z; (iii) -1+x, y, z; (iv) -1+x, -1+y, z;
(v) x, -1+y, z; (vi) 1+x, 1+y, z; (vii) x, 1+y, z; (viii) 1+x, y, z.

Table S3 **Calculated lattice constant information from XRD data for BiNS.**

2 Theta	Lattice distance(Å)	Lattice location
26.138	3.4050	(1 0 1)
32.619	2.7426	(1 1 0)
34.409	2.6043	(1 1 1)
40.902	2.2043	(1 1 2)
46.788	1.9399	(2 0 0)

Table S4 **Calculated lattice constant information from XRD data for BiNS@NaLnF$_4$.**

2 Theta	Lattice distance(Å)	Lattice location
26.604	3.3478	(1 0 1)
32.700	2.7363	(1 1 0)
34.196	2.6199	(1 1 1)
39.201	2.2962	(1 1 2)
46.326	1.9976	(2 0 0)

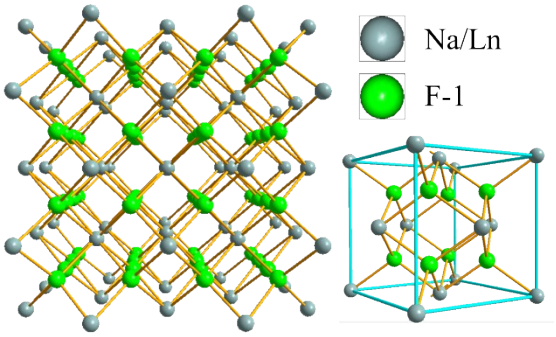

Figure S6 **X-ray diffraction structure analysis of $NaLnF_4$ viewed along the b axis to show the layers stacked perpendicular to the c axis (left), and the view of a cell structure including the coordination geometry (bottom right).**

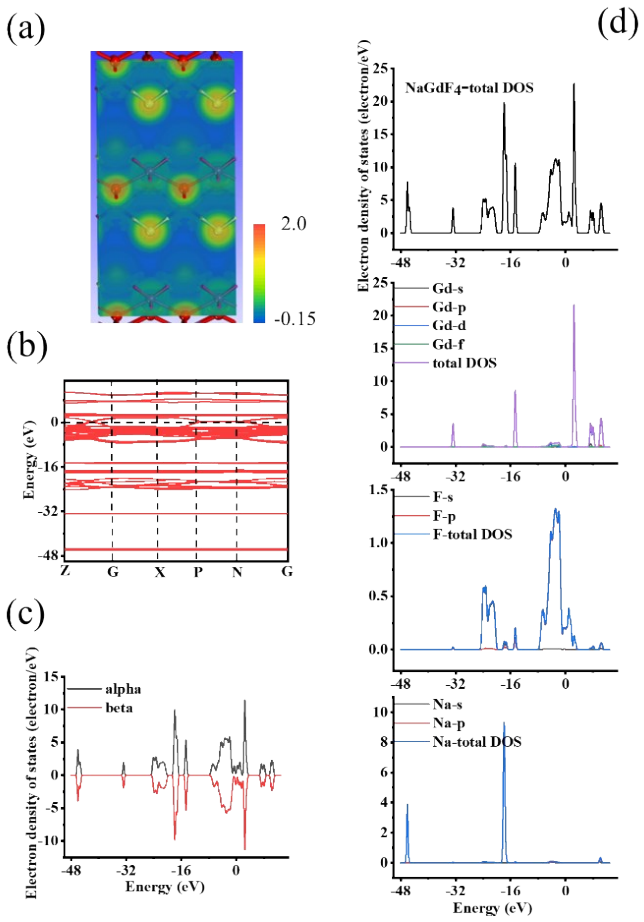

Figure S7 **The DFT structure analysis of $NaGdF_4$.** (a) Electron density map of BiOCl. (b) the DFT of band structure, resulting in $NaGdF_4$ has a conductor prosperity. (c) the total density of states (TDOS). (d) Analyzing the different distribution of elements for DOS.

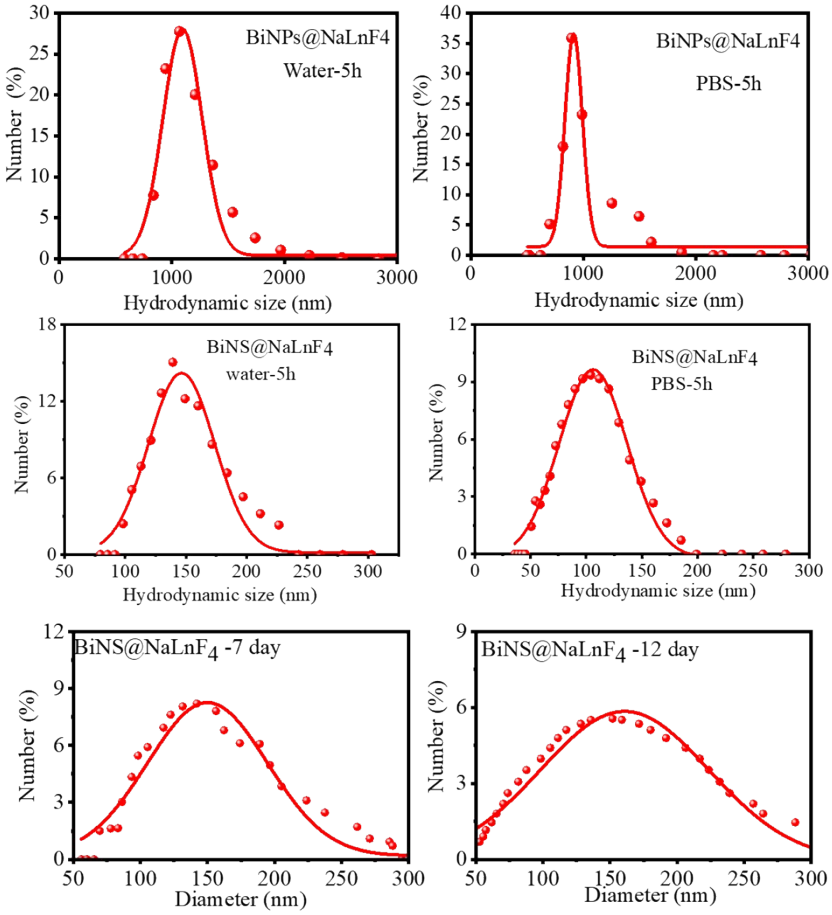

Figure S8 **The hydrodynamic stability of Bi-based samples with different solutions.** Samples were placed in different solution (water and PBS) for 5 h, indicating the good stability of the BiNS@$NaLnF_4$ nanoparticles in different environment over 5 h. A long times hydrodynamic size distribution of BiNS@$NaLnF_4$, demonstrating a good stability during 12 days retaining.

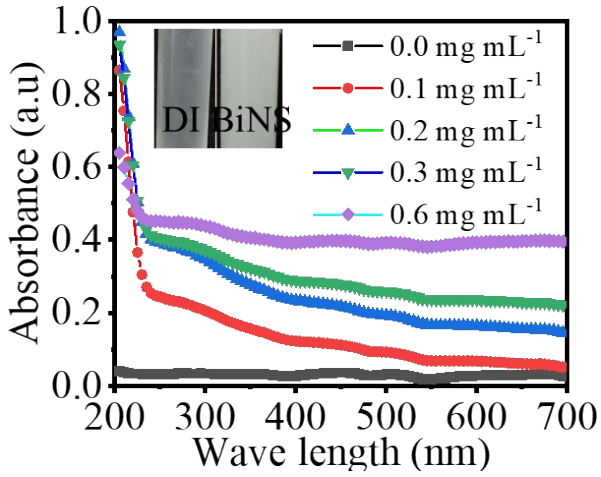

Figure S9 **Extensive UV-vis spectra of BiNS@$NaLnF_4$ at different concentrations.** The spectra suggest a large absorption field in the UV-vis zone. The insert is a photography of a sample in DI.

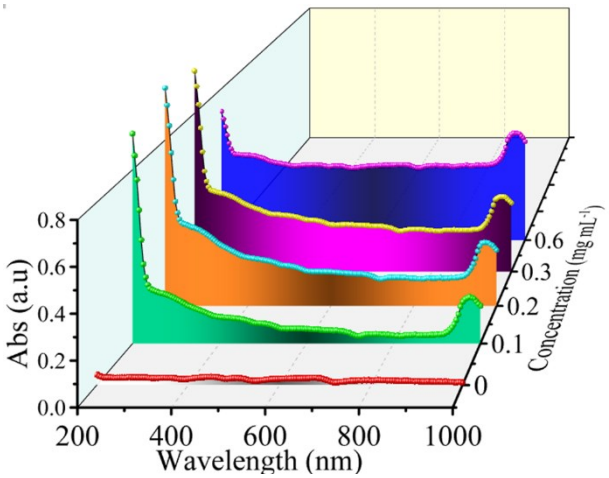

Figure S10 **All of the UV-visible-NIR spectra for the BiNS@$NaLnF_4$ at different concentrations.**

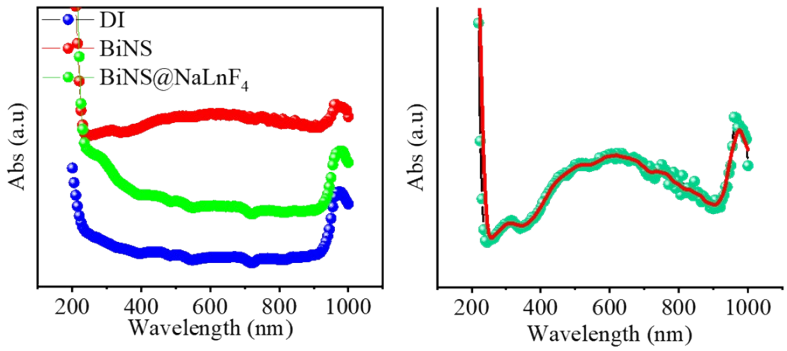

Figure S11 **The UV-Vis-NIR spectra of the DI, BiNS and BiNS@NaLnF$_4$, respectively (Right is BiNS absorption spectrum that illustrate a wide light absorption).**

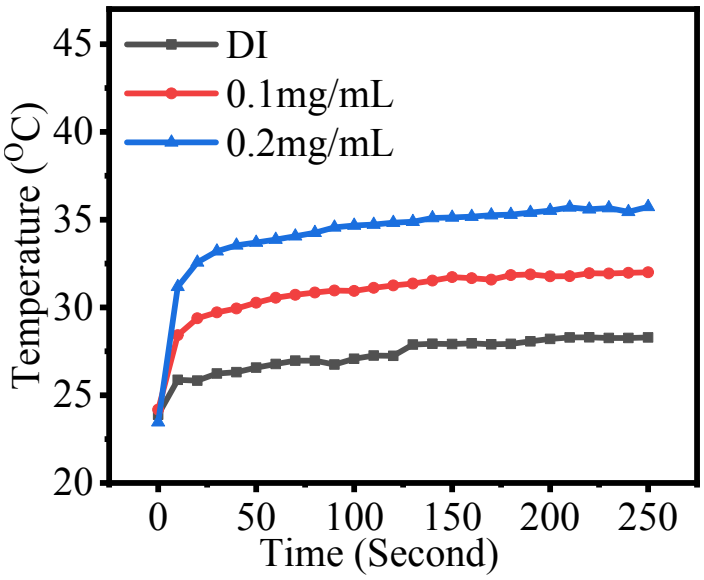

Figure S12 **The photothermal conversion efficiency of the BiNS@NaLnF$_4$ at 980 nm laser irradiation with 0.49 W cm^{-2} and different concentrations.**

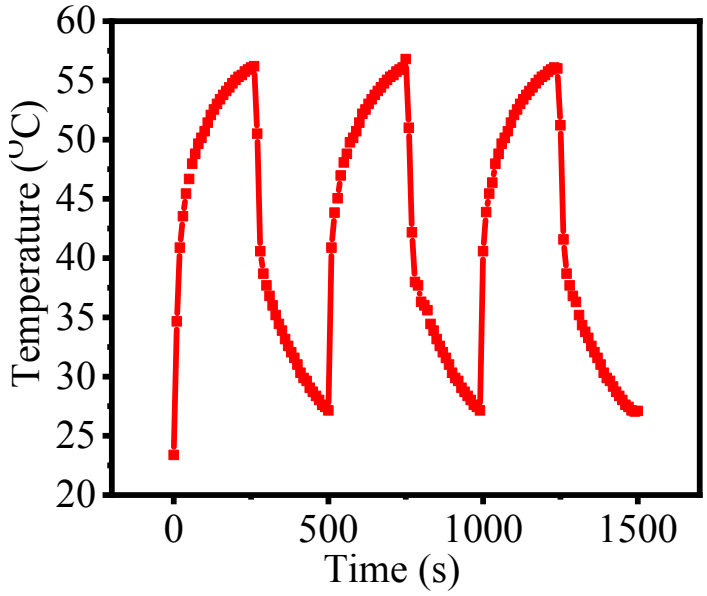

Figure S13 **The photothermal conversion curves for three cycles indicate a good**

sensitivity of the photothermal response.

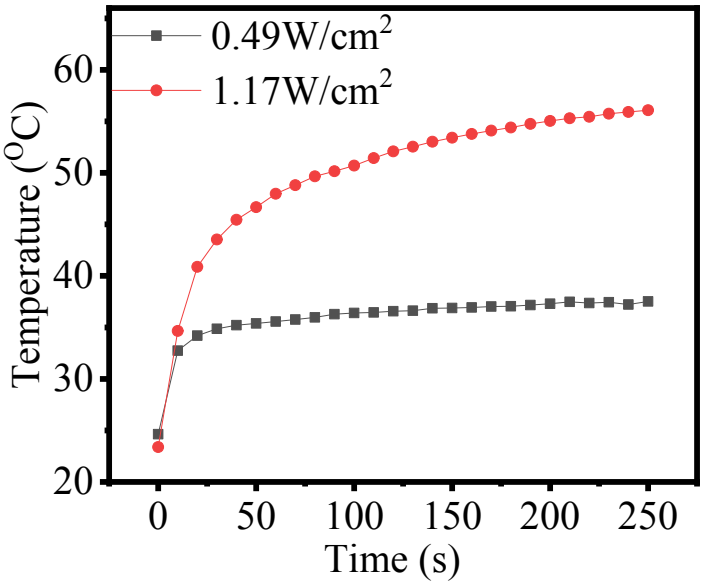

Figure S14 **The photothermal response curves for different power densities at a concentration of 0.2 mg mL^{-1} for BiNS@NaLnF$_4$.**

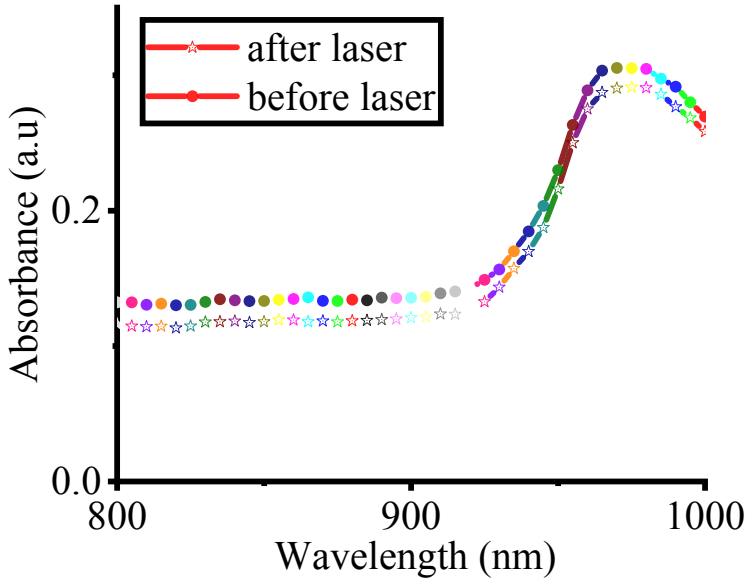

Figure S15 **The UV-vis absorption curves before and after 980 nm laser irradiation at a concentration of 0.2 mg mL^{-1} for BiNS@NaLnF$_4$.**

Table S5. *In vitro* concentration-dependent CT values

Concentration	0mg/mL	1.25mg/m	2.5mg/mL	5 mg/mL	10mg/mL
BiNS@NaLnF$_4$	**-30.5**	**32.5**	**76.3**	**165.2**	**306.1**
	0mg/mL	**0.625mg/**	**1.25mg/**	**2.5**	**5mg/m**
Ioversol	**-30.5**	**-6.7**	**16.7**	**43.3**	**123.9**

Table S6. *In vitro* MRI T1-weighted values

Gd^{3+} Concentration（mM）	**0**	**0.1875**	**0.375**	**0.750**	**1.50**
BiNS@NaLnF$_4$（1/T1）S^{-1}	**0.29886**	**1.44871**	**2.46307**	**4.54477**	**8.83699**

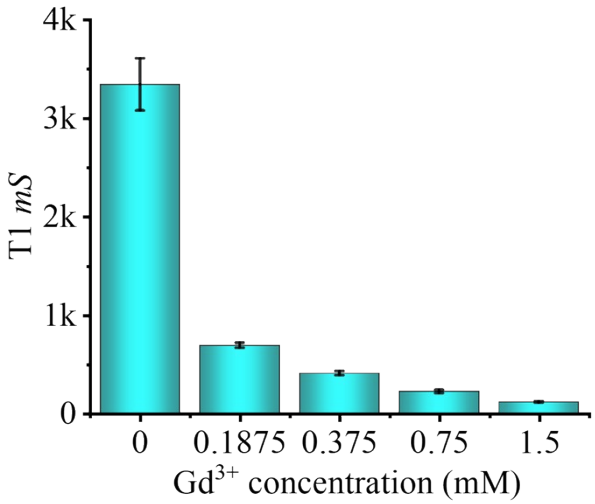

Figure S16 **Change in relaxation T1 time with the concentration of BiNS@NaLnF$_4$. The higher concentration for BiNS@NaLnF$_4$ results in shorter T1 relaxation times in MRI.**

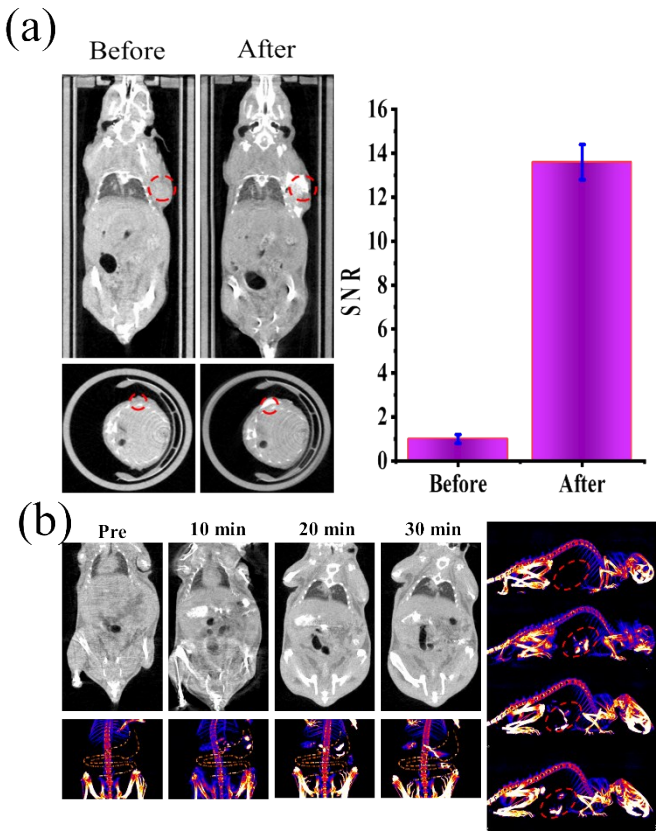

Figure S17 (a) The 2D computed tomography images before and after administration of BiNS@$NaLnF_4$, right is signal-noise ratio for tumor region. (b) Enhanced gastrointestinal imaging function.

Table S7. *In vitro* MRI T1-weighted relaxation times

Gd^{3+} Concentration（mM）	**0**	**0.1875**	**0.375**	**0.750**	**1.50**
BiNS@$NaLnF_4$（T1）mS	**3343.6**	**690.268**	**405.997**	**220.033**	**113.161**

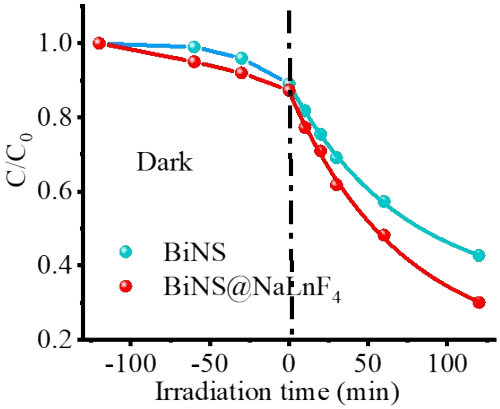

Figure S18 **The degradation ratio of BiNS and BiNS@$NaLnF_4$ under different time vis-light irradiation at concentration of 5 mg mL^{-1}. Indirectly suggest that the heterostructure $NaLnF_4$ loaded BiNS enhance the generation of electrons and holes.**

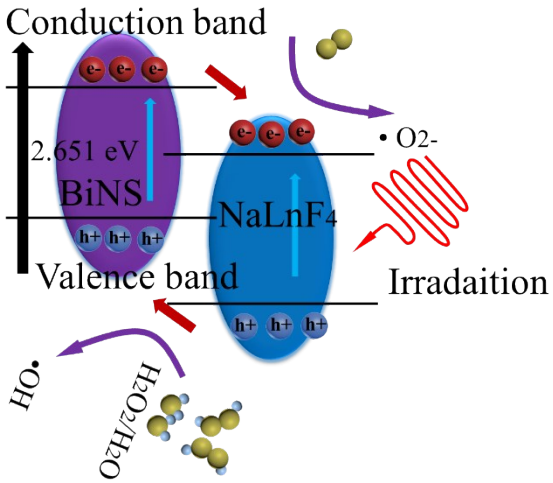

Figure S19 **Demonstration of the MO photodegradation reaction mechanism for BiNS@$NaLnF_4$ results.**

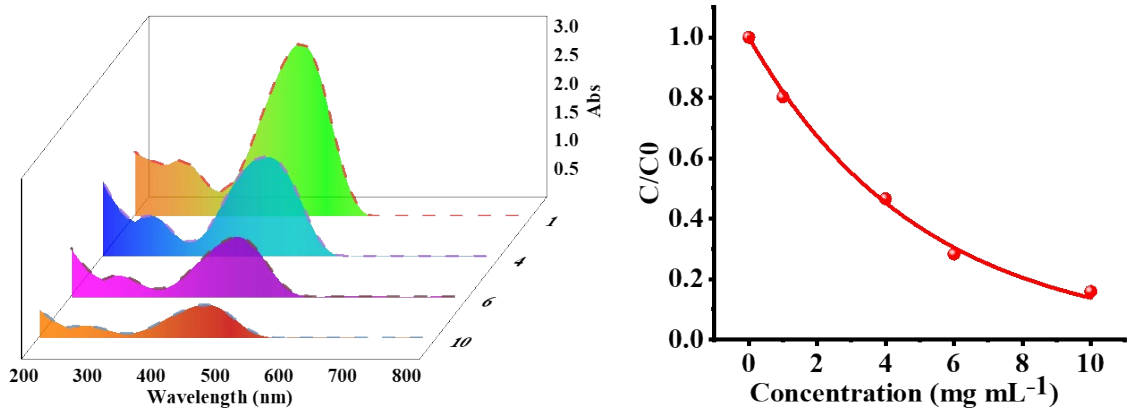

Figure S20 **MO photodegradation reaction ratio of BiNS@NaLnF$_4$ at low pH environment, pH=5 (Left: absorption spectrum of MO degradation at different concentrations within 60 min vis-light irradiation; Right: photodegradation ratio of MO with the different concentrations).**

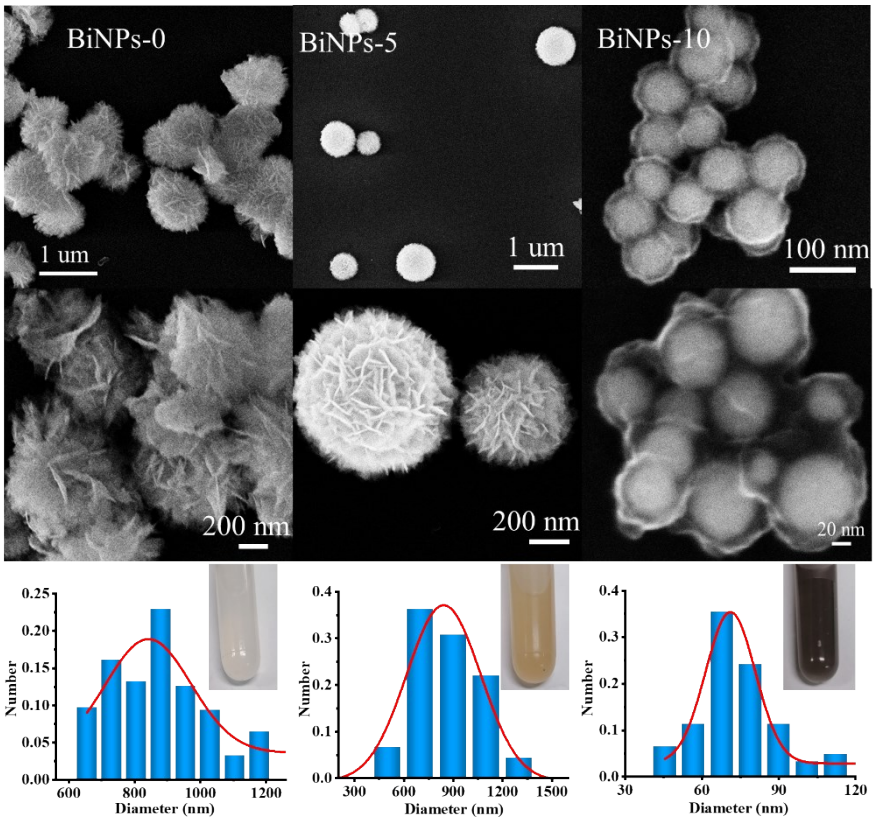

Figure S21 **Controlled synthesis of BiNPs at different H$^+$ concentrations (0, 5 and 10 mL HNO$_3$, respectively); insert photographs of BiNPs-0, BiNPs-5 and BiNPs-10.**

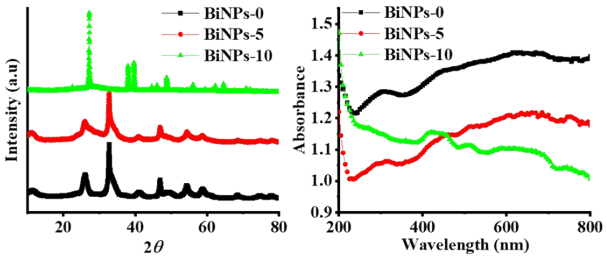

Figure S22 **XRD and UV-vis-NIR spectra analysis of BiNPs at different H^+ concentrations (0, 5 and 10 mL HNO_3, respectively).**

Reference

1. Ren, W.; Yan, Y.; Zeng, L.; Shi, Z.; Gong, A.; Schaaf, P.; Wang, D.; Zhao, J.; Zou, B.; Yu, H.; Chen, G.; Brown, E. M.; Wu, A., A Near Infrared Light Triggered Hydrogenated Black TiO2 for Cancer Photothermal Therapy. *Adv Healthc Mater* **2015,** *4* (10), 1526-36.

2. Liu, Y.; Ai, K.; Liu, J.; Deng, M.; He, Y.; Lu, L., Dopamine-melanin colloidal nanospheres: an efficient near-infrared photothermal therapeutic agent for in vivo cancer therapy. *Adv Mater* **2013,** *25* (9), 1353-9.